Construction and Building Materials 416 (2024) 135073

Contents lists available at ScienceDirect

Construction and Building Materials

journal homepage: www.elsevier.com/locate/conbuildmat

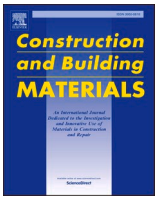

Transport properties of concrete containing lithium slag

Md Tanvir Ehsan Amin *, Prabir Kumar Sarker, Faiz Uddin Ahmed Shaikh

School of Civil and Mechanical Engineering, Curtin University, Perth, Australia

ARTICLE INFO

Keywords:
Lithium slag
Supplementary cementitious material
Workability, Compressive strength
Volume of permeable voids
Water penetration depth
Sorptivity co-efficient
Porosity

ABSTRACT

Lithium Slag (LS), also known as Delithiated Beta Spodumene (DBS), is a by-product of lithium extraction from spodumene ore that contains active silicon dioxide and aluminium oxide making it a potential supplementary cementitious material (SCM) for concrete. This study investigated the transport properties of concrete at 28, 90, and 180 days by incorporating LS as an SCM with cement replacement levels of 20%, 40%, and 60%. The findings reveal that 20% to 40% LS enhanced compressive strength, and reduced permeable voids, water penetration, sorptivity, and porosity, leading to improved transport properties. As LS reacts slowly, 40% LS resulted in 18.34% higher compressive strength at 180 days compared to that of the control mix. Therefore, VPV, water penetration depth, and sorptivity co-efficient of concrete with 40% LS were found 15.96%, 24.79% and 38.46%, respectively, lower than the control mix. In addition, porosity analysis confirmed that with the increase of LS in concrete, porosity decreased over time. Moreover, SEM analysis demonstrated the development of $CaCO_3$ crystals at 40% LS, further reducing porosity. However, beyond 60% cement replacement by LS, a decline in concrete properties was observed due to unreacted LS particles. Therefore, this research underscores the potential use of LS to enhance durability of concrete.

1. Introduction

For centuries, Portland cement has been used as the most common binder for concrete. The remarkable ability of concrete to facilitate the development of infrastructure and architectural projects has made it an integral component of construction worldwide. Due to the significant amount of CO_2 emission caused by cement manufacturing, researchers are exploring alternative materials to replace it. As a result, the use of supplementary cementitious materials (SCM) has become increasingly popular, with some of them now established as commercial products for many decades such as fly ash [1], silica fume [2], steel slag [3,4] and ground granulated blast-furnace slag [5,6]. However, in recent years, extensive research has been conducted to explore the potential utilization of Lithium Slag (LS) as a SCM in the construction industry, particularly in the production of eco-friendly or green concrete. These investigations aim to leverage the properties of LS to develop sustainable construction materials that reduce environmental impact and promote resource efficiency. Studies revealed that, while mixing with cement, LS undergoes a reaction with $Ca(OH)_2$ and generates hydrated calcium silicate (C–S–H) gel. This significantly facilitates the mechanical and durability properties of concrete [7]. Therefore, the utilization of LS as a SCM will potentially improve the basic performance of concrete, reduce the land required for its dumping and help to reduce carbon footprint with substantial economic and environmental advantages [8,9].

Lithium has become one of the most coveted commodities due to its high demand in recent years. This demand is predicted to upsurge significantly in the coming decades. In 2021, a total of around 100,000 metric tons of lithium carbonate was produced globally, where 55% was contributed by Australia. The production is expected to be tripled over the coming decades [10]. However, the major drawback of lithium production is the lithium refinery residue (LRR) or lithium slag known as LS which occupies a considerable area of land, and it may cause environmental issues. It is estimated that one ton of lithium carbonate produces 9–10 tons of LS [11,12]. This huge volume of waste is either stored in dams or thrown into landfills as there is no other way to dispose it. On the other hand, cement is responsible for 8% of the world's carbon dioxide (CO_2) emissions [13]. Therefore, using LS as a supplementary binder can be a feasible way of managing the waste as its potential pozzolanic property has been demonstrated in recent research works [8,14,15]. However, a systematic study to understand the durability properties of concrete containing LS is scarce in literature [16].

Numerous studies have been carried out to explore the effectiveness of LS as a potential SCM and proved that LS can significantly improve mechanical [16,17] and microstructure properties [8,18] of concrete up

* Correspondence to: School of Civil and Mechanical Engineering, Curtin University, Perth, Western Australia 6102, Australia.
E-mail address: m.amin6@postgrad.curtin.edu.au (M.T.E. Amin).

https://doi.org/10.1016/j.conbuildmat.2024.135073
Received 16 October 2023; Received in revised form 21 December 2023; Accepted 15 January 2024
Available online 30 January 2024

to a certain replacement level. Along with other properties, the use of LS is also found to be advantageous in elastic modulus [8], drying shrinkage [7,19], creep [17] and workability [19] of concrete. LS demonstrates effectiveness only within a specific range. For instance, He et al. [17] revealed that with the increase of a certain amount (20%) of LS content shows best result to reduce the drying shrinkage and creep of concrete at later age of curing.

Li & Huang [19] investigated the impact of LS on white Portland cement using a wet-grinding method that basically enhances the early strength development of concrete. The experiment suggests that the use of 5% LS as high-quality raw materials improves the physio-chemical and mechanical properties of white Portland cement. The utilization of LS in Ultra-High-Performance Concrete (UHPC) was also investigated by several researchers and found very effective as well [8,20]. For UHPC, He el al. [8] identified that at early-stage, LS reduces the compressive strength. However, at later age the specimen containing 10% LS exhibited better result by surpassing the strength of control specimen. They concluded that LS shows some pozzolanic activity which is mainly responsible for significant development of the concrete strength at later stage.

Tan et al. [15] used nano-LS slurry to understand the consequence of wet-ground LS on the performance concrete. It is seen that early hydration product is formed by nano-LS slurry which is responsible for the rapid early strength development. In this research, it was also found that, 30 min wet grinding significantly reduces the size of LS. This was shown by the reduction of D(0.5) from 30.38 mm to 3.04 mm. Thus, grinding of LS to smaller particles size promoted the dissolution of aluminate, silicate, and lithium ions of cement that resulted in early strength development of LS blended cement [11,21].

He et al. [22] confirmed that LS can be used as SCM in backfill mining by activating NaOH. Zhai et al. [23] investigated the ionic dissolving characteristics and hydration properties of mixed cement incorporating LS powder which helps to form ettringite at a later stage in the hydrated product. Thus, using LS at proper amount can make the cement paste more compact. However, in few experiments, LS was used as an admixture and it showed some negative effects on workability [7] because of containing zeolites and having higher specific surface area [24].

Very limited research is carried out on the durability of concrete containing LS. Li & Huang [19] concluded that LS significantly improved the pore structure by reducing porosity and increasing compactness of concrete. Qi et al. [14] found that LS significantly decreased the carbonation resistance and chloride penetration over time. However, it was also seen that when water-binder ratio decreased, chloride-ion diffusion coefficient gradually decreased both at 28 days and 84 days [25]. The effect of sulfate attack was also investigated by Li et al. [26] where no severe damage was observed in the specimens containing LS over a period of two years of sulfate exposure.

The alkali-aggregate reaction (AAR) was investigated by Arribas et al. [3]. The authors concluded that, the LS blended concrete did not show excessive expansion. Thus, LS was found effective to reduce AAR by pozzolanic reaction. He et al. [8] performed SEM analysis by magnifying 10,000 times to understand the impact of LS on the concrete specimen. The authors found that initially LS showed less activity by leaving large voids and capillary pores which degraded the microstructure of concrete at early ages. However, at the late ages, the concrete becomes compact leaving no significant CH in the specimen. Most of the pores that were present at the earlier stage are filled by hydration product (C-S-H gel) because of pozzolanic effect of LS. Similar results are also reported by other researchers [11,16,20].

A wide range of research have been carried out in terms of physio-chemical test, mechanical properties, fresh properties, micro and nano-structural properties of concrete containing LS. However, very limited literature can be found on the durability properties of LS blended concrete, especially on the transport properties. Therefore, this study aims to investigate the durability of LS blended concrete, including volume of permeable voids (VPV), water penetration depth, sorptivity and SEM analysis.

2. Materials and methods

2.1. Materials

In this study, ordinary Portland cement (OPC) was used as the primary binder and lithium slag (LS) was used as supplementary cementitious material. The cement conforms to the quality requirements specified in the ASTM C150 and Australian standard AS 3972:2010 as type I cement. The LS was supplied by local lithium refinery in Western Australia. Before using, the LS was oven-dried at $105 \pm 5\ ^{\circ}C$. LS particles are mostly irregular in shape including flaky particles compared to cement as found in the scanning electron microscopy (SEM) image shown in Fig. 1. The chemical compositions of the cement and LS are given in Table 1. A comparison of cement and LS is presented in Fig. 2 by a ternary diagram that graphically represents the SiO_2-CaO-Al_2O_3 compositions of these materials. It is clearly perceived that LS contains higher percentage of SiO_2 and Al_2O_3 compared to OPC used in this study. Furthermore, X-ray diffraction (XRD) analysis was conducted to determine the mineralogical characteristics of LS and OPC as depicted in Fig. 3. Calcium fluorite (CaF_2) was incorporated with the samples as reference material and the obtained data was analysed using EVA software. Therefore, the peaks corresponding to CaF_2 in the spectrum do not originate from the binding materials. Table 2.

In this study, natural sand was used as fine aggregate (FA) while crushed granite was used as coarse aggregate (CA) with a maximum size of 20 mm. The particle size distribution of FA and CA is presented in Fig. 4 and basic properties of FA and CA are presented in Table 3. All materials were sourced from local suppliers in Western Australia. Before casting, both fine and coarse aggregates were soaked in clean water for at least 24 h and then air-dried to achieve a saturated surface dry (SSD) condition according to the Australian Standard AS 1141.3.1 (2012). Normal tap water was used to mix the concrete.

2.2. Concrete mix proportions

In this research, a total of four concrete mixes were prepared to conduct all testing including compressive strength test, volume of permeable voids (VPV), water permeability and sorptivity. In the first mix, concrete specimens were prepared without any LS content which is denoted as control mix. The subsequent mixes involved the utilization of cement and lithium slag, with varying proportions of 20%, 40%, and 60% LS replacing the cement. The mixing was carried out in a pan mixture, wherein the binding materials and aggregates were first mixed for 3 min in a dry condition. Subsequently, water was cautiously added and mixed until a uniform mixture was achieved. Rheobuild 1000 superplasticizer was used in mixtures 40LS and 60LS to achieve workability with a consistent water-to-binder ratio of 0.43. The mixture proportions are given in Table 4. After mixing the concrete, slump tests were performed to determine the workability and the slump values for all mixes are also presented in Table 4. 100 mm in diameter by 200 mm in height cylindrical moulds were filled and compacted properly in two layers to avoid any honeycombs or voids. To maintain consistent quality, all the mixes in this study were prepared under identical conditions. The specimens were demolded after 24 h and cured in lime water until the designated testing days.

2.3. Experimental methods

This study evaluated the compressive strength and transport properties of concrete using a series of experiments. Hence, 20%, 40% and 60% cement is replaced by LS and the results are compared with those of the control concrete. To gain a comprehensive understanding on the durability performance, VPV, water permeability and sorptivity tests

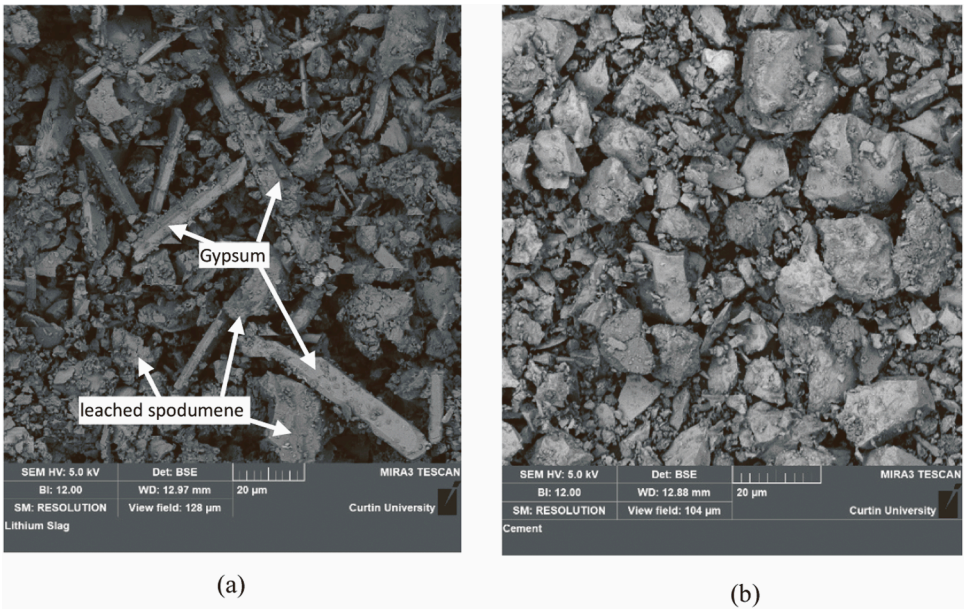

Fig. 1. SEM image of (a) LS and (b) OPC.

Table 1
Oxide compositions of cement and lithium slag (mass %) [27].

Oxide	SiO_2	Al_2O_3	Fe_2O_3	CaO	MgO	SO_3	K_2O	Na_2O	LOI
Cement	20.70	5.70	2.90	63.10	1.30	3.30	0.40	0.30	1.90
LS	54.53	21.08	1.45	7.535	0.575	5.62	0.884	0.72	6.76

were conducted along with compressive strength test of all four mixes. The summary of the experimental program is presented in Table 5.

2.3.1. Workability and compressive strength test

The workability of freshly mixed concrete was assessed through a slump test and the compressive strength for all mixes were determined at 7, 28, 90 and 180 days where at least three cylinders of 100 × 200 mm were prepared for each mix and each test day. To evaluate the concrete's compressive strength, a consistent loading rate of 0.33 MPa/s was maintained in accordance with ASTM C39 standard. Table 4 displays the results obtained from the slump test of all concrete mixtures.

2.3.2. Volume of permeable voids (VPV)

The VPV test is crucial for assessing concrete's permeability, durability, and resistance to water penetration and in this study, VPV test is performed according to the ASTM C642 standard. Cylindrical concrete specimens measuring 100 ϕ mm × 200 mm were cut into three 50 mm thick disc samples using central part except top and bottom 25 mm thick concrete layers. Each disk is then oven dried (OD) at 110° ± 5 °C for at least 24 h. Then the weights are recorded until two consecutive measurements showed a difference of less than 0.5%. After that, the samples were submerged in water at 21 °C for at least 48 h to achieve saturated surface-dry (SSD) condition. Subsequently, the samples were boiled in water for 5 h and cooled naturally for approximately 14 h. The weight of the specimens at the state of boiled SSD was measured. After immersion and boiling, the samples were suspended in water to ascertain their apparent mass. To obtain the mean value a minimum of three samples were tested. Furthermore, the void percentage was calculated using Equation 1:

$$\text{Volume of permeable voids } (\%) = (B - A)/(B - C) \times 100 \quad (1)$$

where A = the mass (in grams) of the OD specimen, B = mass (in grams) of the SSD sample in air after immersion and boiling and C = apparent mass (in grams) of the sample after immersion and boiling.

2.3.3. Sorptivity

The sorptivity tests of concrete samples were conducted following ASTM C1585 standard. Cylindrical specimen (100 ϕ × 200 mm) were cut into three 50 mm thick disc samples using the central part except the top and bottom 25 mm thick concrete layers. The samples were then stored in a controlled chamber where 50 ± 2 °C temperature and 80 ± 3% relative humidity is maintained for three days. After that, all samples are kept in a sealable container at 23 ± 2 °C for 15 days. After conditioning, the specimens were removed and prepared for testing. All surfaces were sealed except the bottom surface which were immersed under water. A pan was filled with tap water and all samples were immersed to a depth of 1–3 mm as depicted in Fig. 5. The initial sorptivity data was recorded at intervals of 0, 1 min, 5 min, 10 min, 20 min, 30 min, 1 hr, 2 hr, 3 hr, 4 hr, 5 hr, and 6 hr.

2.3.4. Water permeability test

Three cylinders with a dimension of 100 ϕ × 200 mm for each mix were placed in the water penetration depth measurement apparatus as shown in Fig. 6. The bottom of the cylinders was sealed properly to confirm water tightness while fixing in the apparatus and a constant pressure was applied maintaining 500 ± 50 kPa for 72 h. After removal, the cylinders were split into two equal pieces and marked the water penetration depth following the BS EN 12390–8 standard.

2.3.5. Thermogravimetric analysis (TGA)

In this study, TGA was conducted to understand the pozzolanic activity of LS by determining the calcium hydroxide (CH) contents in concrete at different LS dosages. The experiment involved measuring weight changes as the temperature varied in a controlled atmosphere. This process simultaneously measured the weight loss due to the decomposition of various phases. A platinum crucible containing 20 mg

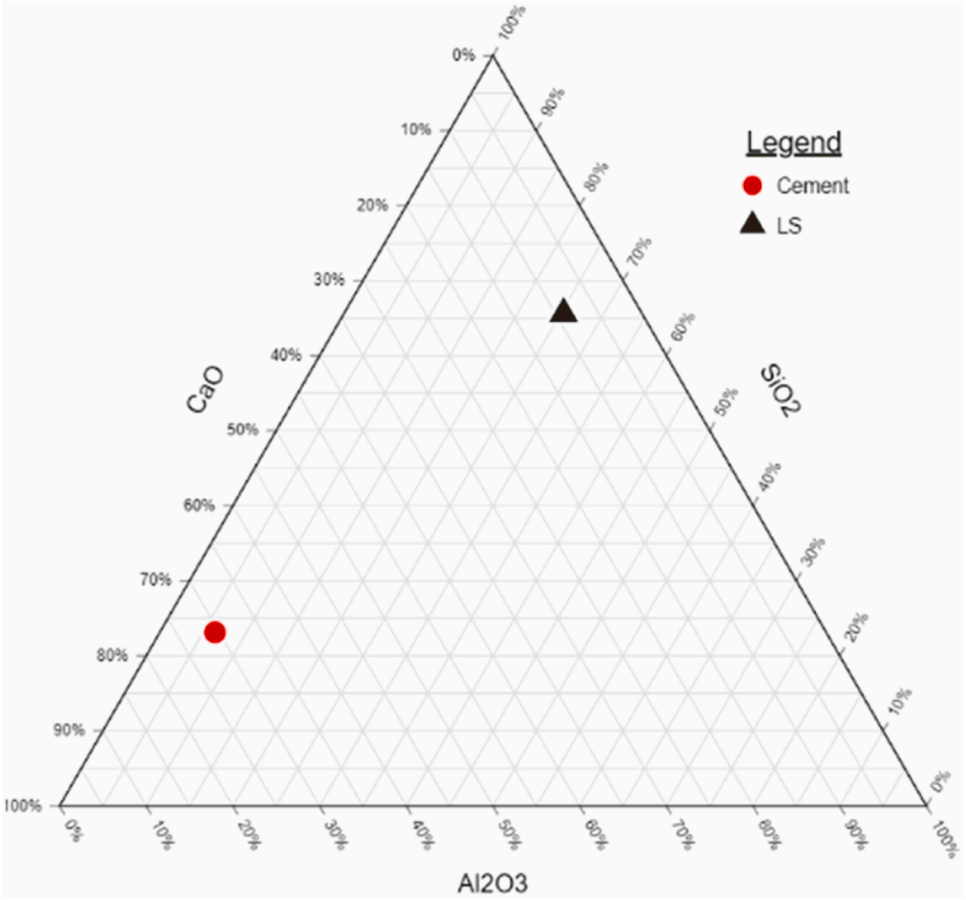

Fig. 2. Ternary diagram of the chemical composition of OPC and LS.

of powdered sample in 110 μL was heated from ambient to 1000 °C at a rate of 10 °C per minute in a nitrogen atmosphere flowing at 100 ml per minute. Data on mass and temperature variations were collected as a function of the furnace temperature. This analysis allows to estimate the amount of CH for control, 20LS, 40LS and 60LS mixtures.

The weight loss of mortar samples at 180 days that occurs during dehydroxylation of CH can be detected from TGA analysis in the temperature range of 400 to 500 °C [28]. Based on Taylor's formula, the CH content is calculated from the weight loss in each sample using Eq. 2 [29].

$$CH(\%) = WL_{CH}(\%) \times \frac{MW_{CH}}{MW_{H_2O}} \quad (2)$$

where, WL_{CH} is the weight loss during the dehydration of CH as percentage of the ignited weight, MW_{CH} and MW_{H_2O} are the molecular weights of CH and H_2O, respectively.

2.3.6. Porosity

During the study, the TBitmap software was used to examine the porosity of concrete samples. Ten micrographs were taken from various sections of the concrete specimens and then processed using the TBitmap software. The micrographs were captured using an optical microscope with 100 times magnification. The software used flood fill algorithm to determine the connected components and resin colour analysis by identifying pixels in the image to perform a quantitative analysis of the porosity. Fig. 7 shows an analysis screen using TBitmap software for a surface image. The pores were categorized into three different sizes according to Abousnina et al. [30] and Awedat et al. [31]. The micropores which are less than 0.32 μm, the mesopores are between 0.2–30 μm, and the macropores are greater than 30 μm. All the micrographs were captured immediately after the compression test.

3. Results and discussion

3.1. Effect of LS on the workability of concrete

The slump values of different mixtures are given in Table 4. It can be observed that the slump value decreased with the increase of LS content in the concrete. The variation of slump value in different mixes are shown in Fig. 8. To maintain the workability, superplasticizer was used in mixtures 40LS and 60LS. The slump value of 20LS, 40LS, and 60LS concrete mixtures were 100, 95 and 90 mm respectively for a constant water/binder ratio of 0.43. Due to high particle porosity along with flaky and angular particles, LS absorbs more water than the cement during mixing, as reported previously [32]. This is considered as a reason for lower workability of concrete with the increasing of LS content in this study.

3.2. Porosity

The study encompasses a comprehensive analysis of the surface porosity of LS blended concrete samples of various mixtures, presenting the findings based on three specific pore categories as shown in the Fig. 9 (a-d). Cementitious materials are known to comprise three distinct pore types. These include gel pores, which are characterized as micropores that has least influence on the strength of concrete [33]. Thus, the contribution of the gel pores to the overall porosity of LS blended concrete can be considered insignificant. It has been observed from Fig. 9(c) that at early days of curing, the microporosity of concrete decreased with the increase of LS. At 28 days, the microporosity of control, 20LS,

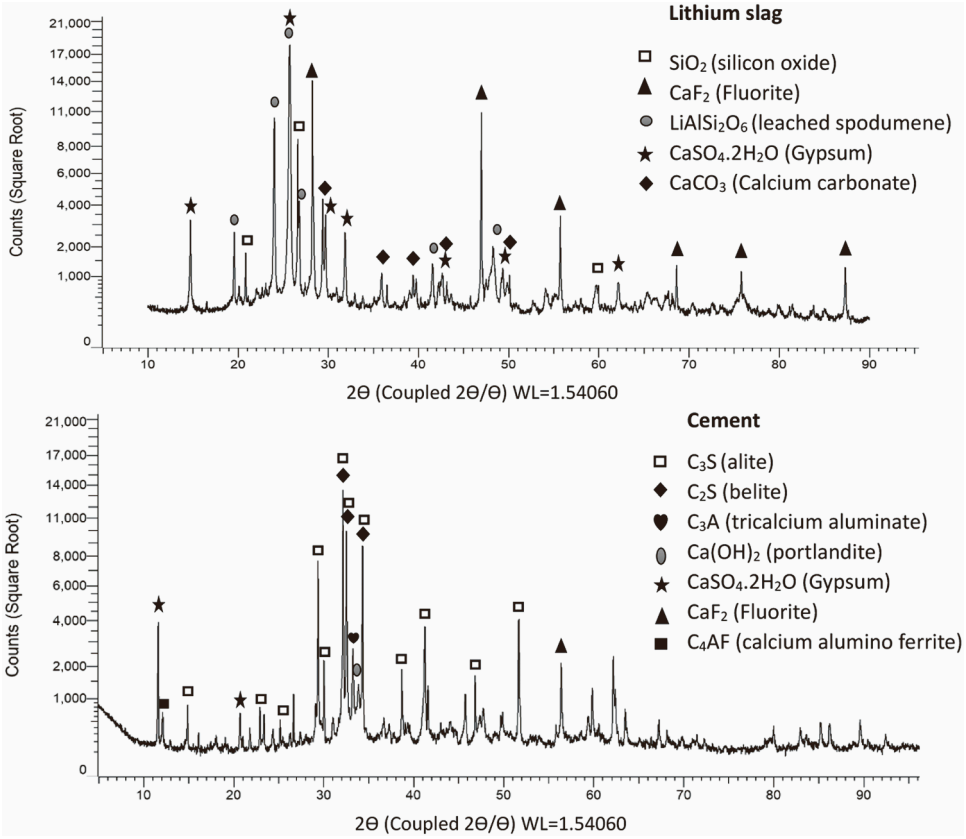

Fig. 3. XRD of LS and OPC.

Table 2
Properties of cement and LS.

Properties	Cement	Lithium slag
Surface area	360 kg/m^2	340 kg/m^2
Median particle size	17 μm	38 μm
Specific gravity	3.1	2.46

40LS and 60LS specimens were 9.8%, 9.48%, 8.3% and 8.29%, respectively. This gradual decrease in microporosity indicates that the smaller particles of LS initially act as a filler material in the early days. Furthermore, at 180 days the microporosity decreased to 9.18%, 8.04%, 8.1% and 7.11%, respectively for all four mixes due to the formation of C-H-S gel in the pores.

Capillary pores, classified as mesopores, having an average radius ranging from 0.32–30 μm, attributed to deliberate air entrainment. However, the macropores which are greater than 30 μm are formed due to inadequate compaction in concrete. In LS blended concrete, the unreacted LS particles also contributed to the pore structure which was reported in other studies [17]. Kumar et al. [33] suggests that the capillary and larger pores are responsible for the variation in strength and transport properties of concrete. He et al. [17] also suggest that at early age, the capillary and larger pores increased with the incorporation of LS into the concrete. In this study, few LS particles were observed in the 20LS, 40LS and 60LS concretes at 28 days. These particles mostly served as filler and had not yet reacted which is observed in SEM images shown in Fig. 19. This suggests that these unreacted LS particles are responsible for creating capillary pores in the concrete that reduced strength at early days of curing. For instance, at 28 days, the 20LS, 40LS,

Table 3
Basic properties of FA and CA.

Properties		FA	CA	Unit
Specific gravity	:	2.62	2.72	-
Water absorption	:	0.6	0.5	%
Bulk density (compacted)	:	1630	1560	kg/m^3
Max aggregate size	:	4.75	20	mm

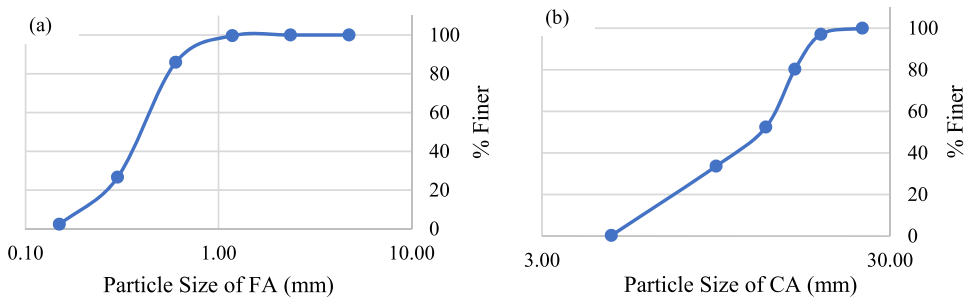

Fig. 4. Gradation curves of FA (a) and CA (b).

Table 4
Concrete mix proportions and slump values.

Mixture	Description	Binder		Water (kg/m^3)	Aggregate		w/b	Slump (mm)	Superplasticizer
		Cement (kg/m^3)	LS (kg/m^3)		CA (kg/m^3)	FA (kg/m^3)			
Control	100% cement is used as binder	426.6	-	185.2	1260.9	724.6	0.43	110	-
20 LS	20% cement replaced by LS	341.3	85.3	185.2	1260.9	724.6	0.43	100	-
40 LS	40% cement replaced by LS	255.96	170.64	185.2	1260.9	724.6	0.43	95	0.5% of binder
60 LS	60% cement replaced by LS	170.64	255.96	185.2	1260.9	724.6	0.43	90	1.3% of binder

Table 5
Summary of experimental program

Property	Code/ Specification	Size of samples	No. of samples	Test days
Compressive strength test	ASTM C39	100 × 200 mm cylinder	Control (3), 20LS (3) 40LS (3), 60LS (3)	7, 28, 90 and 180 days
Volume of permeable voids	ASTM C642	100 × 50 mm cylindrical disc	Control (3), 20LS (3) 40LS (3), 60LS (3)	28, 90 and 180 days
Sorptivity	ASTM C1585	100 × 50 mm cylindrical disc	Control (3), 20LS (3) 40LS (3), 60LS (3)	28, 90 and 180 days
Water permeability	BS EN 12390-8	100 × 200 mm cylinder	Control (3), 20LS (3) 40LS (3), 60LS (3)	28, 90 and 180 days

Fig. 5. Sorptivity test of concrete.

Fig. 6. Water penetration depth test setup.

and 60LS concretes consist of 5.76%, 6.2%, and 6.4% macropores, respectively whereas control concrete consists of 5.3% macropores. Furthermore, the pore greater than 0.2 μm increased by 8.27–9.51% with the increase of LS content from 20 to 60% in the concrete at an early age. However, at later age, the percentage of mesopores along with the percentage of macropores decreased with the increment of LS into concrete. This reduction is consistent with up to 40% replacement of cement by LS. Compared to the control mix, the mesopores and macropores of 40LS concrete decreased by 26.5% and 42.5%, respectively. Therefore, the total porosity of 40LS concrete also decreased by 20.2% than that of control concrete after 180 days. This trend also supports the findings of other transport properties as explained before. In contrast, 60LS concrete consists of around 32.5% and 10% higher macropores and mesopores, respectively than 40LS concrete. Therefore, the strength and transport properties showed degrading trends when using more than 40% LS in the binder.

3.3. *Effect of LS on the compressive strength of concrete*

The long-term durability of concrete is influenced by its compressive strength because higher compressive strength typically translates to compact microstructure and hence, greater resistance to penetration of aggressive substances. Fig. 10 shows how LS affects the compressive strength over time. It has been observed that with the increase of LS into concrete, the compressive strength of concrete decreased at early age. For instance, the compressive strength of control specimens is the highest among all the mixes at 7 days and the 20LS, 40LS, and 60LS concrete specimens show 12.4%, 26.5%, and 49.4% lower compressive strengths, respectively than the control specimen. This indicates that the pozzolanic reaction of LS at the early stage is slower which mainly depends on the availability of calcium hydroxide (CH). By replacing cement with lithium slag, the amount of CH is decreased, consequently slowing down the initial progression of compressive strength. Furthermore, lithium slag particles are flaky and of irregular shape as shown in Fig. 1 which may create pores in the matrix. Additionally, it also has a smaller surface area compared to cement particles, which limits chemical reactions and bonding, leading to lower strength development during the early stages of curing.

At 28 days of curing, the compressive strength of 20LS, 40LS and 60LS concrete were 42.04, 41.35 and 40.87 MPa respectively, which are 6.4%, 7.9% and 9% lower than that of control specimen. However, the LS replacement level shows significant compressive strength growth over time. The compressive strengths of 20LS, 40LS, and 60LS concretes improved significantly from 7 to 90 days of curing, followed by a consistent rate of strength improvement thereafter. At 6 months, the LS concrete reaches about 56, 61 and 53 MPa which are about 61%, 107% and 167% higher strength developments than the early days of curing,

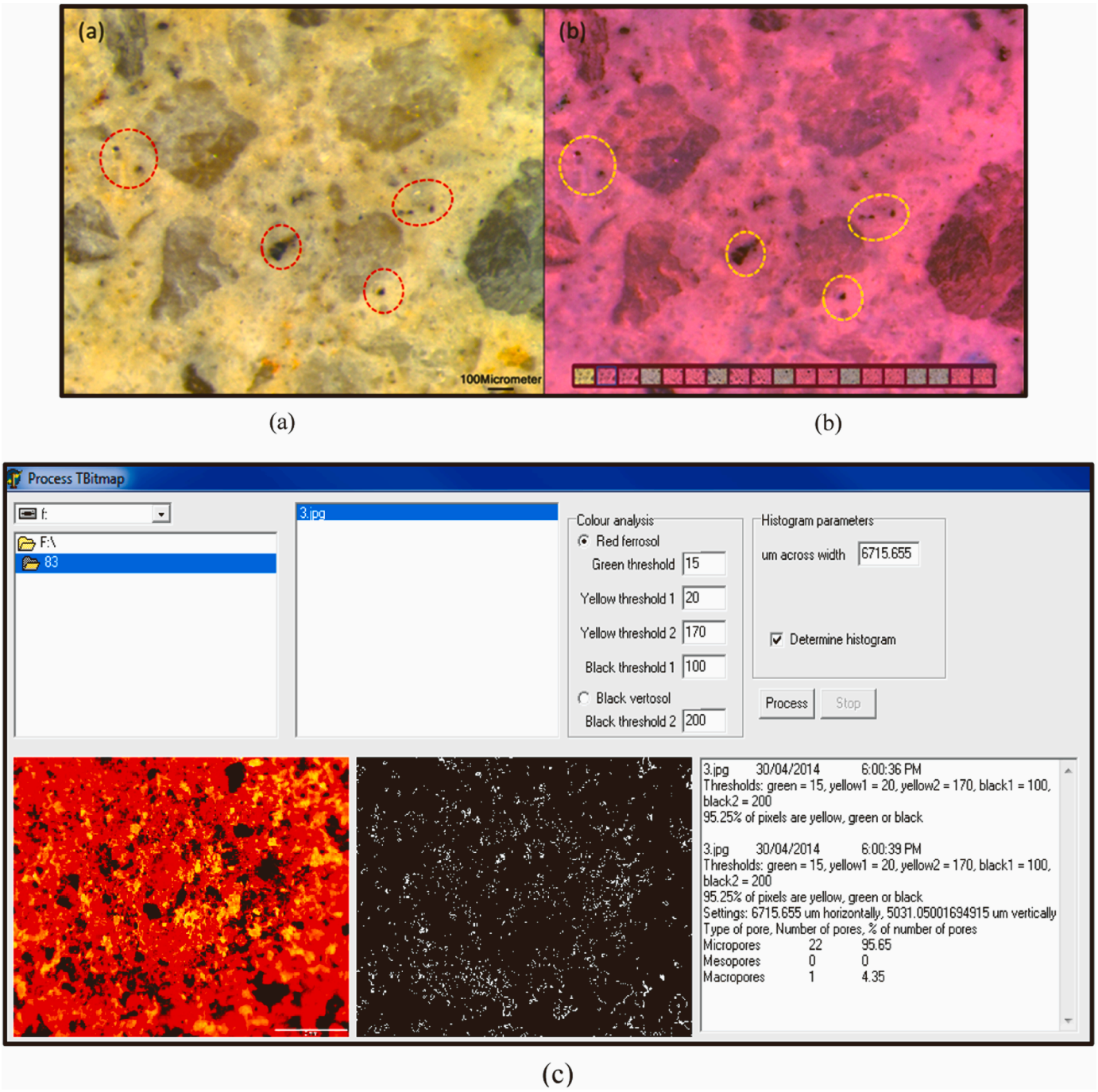

Fig. 7. Analysis using TBitmap software (a) natural colour of the surface, (b) readjusted colour to be readable by the software and (c) analysis screen of TBitmap.

while the control concrete shows only 29% compressive strength growth compared to 7 days of age. LS particles exhibit high reactivity at a later stage with calcium hydroxide (CH) and form additional C-S-H (calcium silicate hydrate) gel. It is also evident that LS has a higher content of SiO_2 and Al_2O_3, making it more reactive with age [27]. By replacing cement with LS, the reactive SiO_2 and Al_2O_3 in the LS promote the formation of C-S-H gel which leads to improved strength development at later ages [1,2]. However, among four mixes, 40% LS content imparts highest compressive strength after 6 months of age. This result supports the findings in the porosity analysis as depicted in Fig. 9. The porosities are calculated based on the analysis using TBitmap software which has been discussed earlier. Previous studies [30,34] demonstrated that the development of compressive strength is significantly influenced by its porosity and it has been observed that the larger pores in concrete have a greater effect on its strength than smaller pores. Fig. 11 displays the relationship of the compressive strength of concrete with the macro-pores at LS percentages of 0%, 20%, 40% and 60%. The macro-porosity of 40LS concrete decreased to 1.7% at 180 days of age which is the lowest among all four mixes. The reduction in large pores (>30 μm) leads to the denser structure and, therefore, improved the compressive strength of 40LS concrete. However, as expected, further addition of LS did not increase the compressive strength even after 6 months of age. LS content of 60% showed 11.5% lower compressive strength than 40LS concrete due to the lower amount of calcium content in the mix. The results of TGA were used to determine the CH contents of the mixtures using Eq. 2. The CH contents of control, 20LS, 40LS and 60LS mixtures

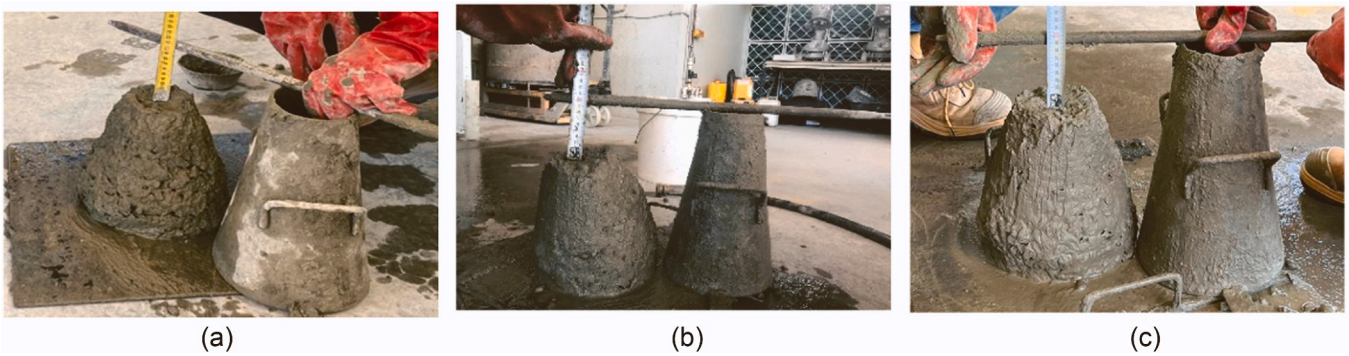

Fig. 8. Slump of LS concrete (a) 20LS, (b) 40LS and (c) 60LS.

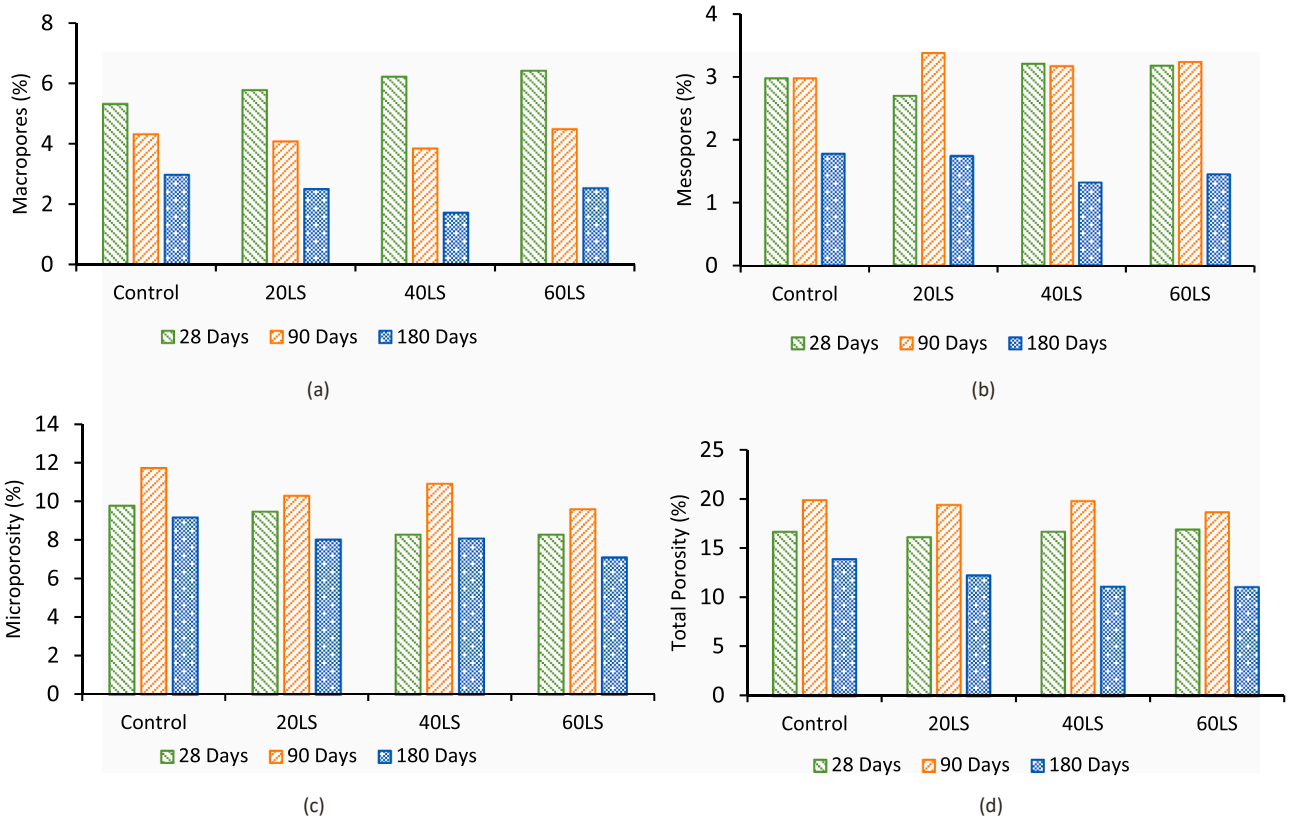

Fig. 9. Porosity of concrete (a) macropore, (b) mesopore, (c) micropore and (d) total porosity.

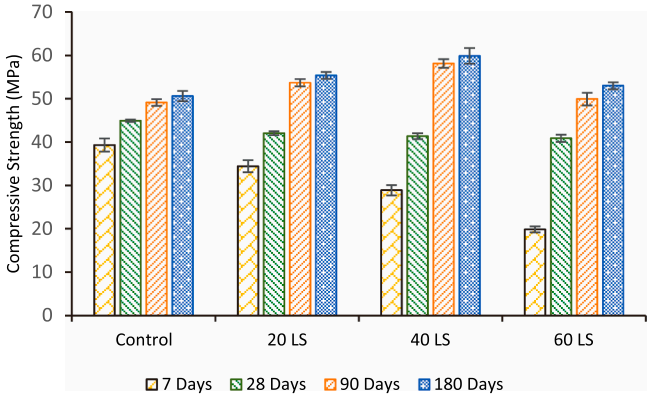

Fig. 10. Compressive strength of different mixes of concrete.

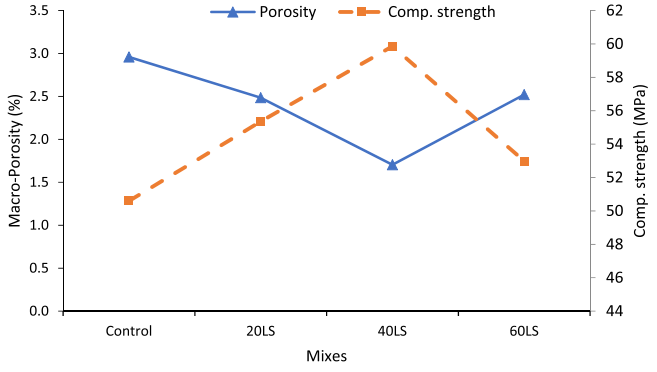

Fig. 11. Compressive strength vs macroporosity at 180 days.

were found 3.87%, 2.82%, 2.63% and 1.99%, respectively. This shows that, 60LS concrete had the lowest CH content available for pozzolanic reaction among all the four mixtures, which is consistent with its low compressive strength. Thus, the use of 40% LS is considered optimum in terms of the porosity and compressive strength of concrete.

3.4. Effect of LS on the VPV of concrete

The VPV is a prominent durability index to assess the permeability of concrete. It refers to the total volume of interconnected pores through which fluids such as air or water can pass. In this experiment, VPV was determined at 28, 90, and 180 days of age for all four mixes and the comparisons are presented in Fig. 12. It is observed that the VPV at early ages tends to increase as the LS content increases. At 28 days, the VPV of the control, 20LS, 40LS, and 60LS concretes were 9.4%, 10.3%, 10.7% and 11.1% respectively. This suggests that at early curing ages, the VPV values of the LS concrete specimens were greater than those of the control specimen, which is consistent with the results found in the compressive strength of those mixes. As the pore volume increases, the compressive strength of concrete decreases at initial stage of curing. As a result, concrete with LS exhibits lower compressive strength than the concrete without LS at 28 days, as shown in Fig. 10.

At 90 days, the VPV for all four mixes did not show any significant changes. Although, the average VPV value at 90 days are appeared slightly higher than those of 28 days, the error bar illustrates that the upper VPV value at 28 days is greater than the lower value at 90 days for all mixes. However, the VPV value of all four mixes significantly decreased with the increase of LS content in the concrete sample at 180 days. According to VicRoads specification [35], VPV value less than 11% is considered to be of excellent quality. Hence, all the mixes studied in this research can be classified as excellent-quality concrete. Compared to the early age, the VPV of control, 20LS, 40LS, and 60LS concretes is decreased by 7.1%, 19.9%, 31.3%, and 24.6%, respectively at 180 days. Hence, 40LS concrete has the least VPV value and the control mix has the highest VPV value at 180 days. The reason behind the lower VPV can be ascribed to the pozzolanic reaction of LS which helped to form a dense microstructure that has been discussed in the microstructure analysis section. As shown in Table 1, LS has higher SiO_2 and Al_2O_3 contents than cement. It is also evident that the presence of amorphous silica and alumina reacts with portlandite to form calcium silicate hydrate (C-S-H) gel. This plays a vital role in enhancing the pore structure as shown in Fig. 13. Furthermore, the results of VPV correlates well with the compressive strengths. A decrease in porosity corresponds to an increase in compressive strength, which is attributed to the greater compactness of the matrix. Therefore, like compressive strength, 40% replacement of cement by LS has shown optimum VPV among all the mixes. As the percentage of macropore decreased to 1.7% which is

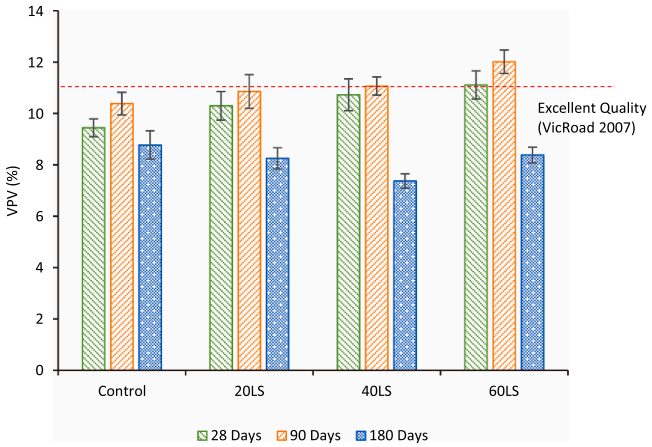

Fig. 12. Volume of permeable voids.

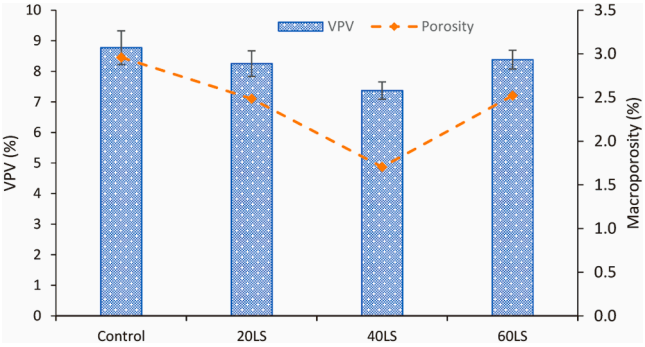

Fig. 13. VPV vs macro-porosity of concrete at 180 days.

lowest among the four mixes, the VPV also decreased to 7.37% at 180 days which is the least among all mixes. However, the total porosity along with the macropore and mesopore increased after 60% replacement of cement by LS, which has been already discussed in the porosity section. Thus, VPV also increased to 8.38% in 60LS concrete. In addition, the use of 60% LS left unreacted LS particles due to lack of $Ca(OH)_2$ content, which is also observed in microstructure analysis.

3.5. Water penetration depth of concrete

The water permeability test determines the resistance to water penetration of concrete under constant water pressure for a certain period. It is an important durability index that evaluates the transport properties of concrete and its resistance to the ingress of water, moisture, and potentially harmful substances such as chlorides or sulfates. The water penetration depth of all mixes after split test are presented in Fig. 15 (a-l) and the results are plotted in Fig. 14 (a). It can be seen that the water penetration depths align with the trend of the VPV test results as depicted in Fig. 14 (b). Fig. 15.

Fig. 14 (a) shows that using LS resulted in an increase in the water penetration depth during the early stages of curing. The increased amount of lithium slag in the concrete mixture is correlated with this rise in water penetration depth.

However, the relationship between LS content and water penetration depth changed at later stages, suggesting that higher proportions of LS in the mix contributed to decrease water penetration depth up to 40% LS content. This effect becomes prominent after 6 months of age. Compared to the water penetration depth observed at 28 days, the 20LS concrete, 40LS concrete, and 60LS concrete exhibited reductions of 23%, 36%, and 20% respectively, at 180 days. The corresponding decrease of water penetration in the control specimen was only about 6%. It is possible that the pores of LS blended concrete are filled up with the secondary C-S-H gel and, therefore, reduced the water penetration depth at a later age. Among all four mixes, 40% LS was found to be the most effective and showed the least permeability in the concrete due to the reduction in porosity as shown in Fig. 14 (c). Gel pores and macropores which are more than 0.2 μm in diameter in concrete play a significant role in water penetration [33,36]. With the use of 40% LS, the total porosity was found to be the lowest which plays a vital role in transporting water through the pores. This result also correlates with the VPV results. Finally, it can be concluded that concrete with LS produced satisfactory results and the trend of the water penetration results is consistent with the VPV, porosity and compressive strengths of the concrete.

3.6. Effect of LS on the sorptivity of concrete

To understand the water absorption of concrete through capillary action, sorptivity is one of the critical measures of concrete study. A higher sorptivity level indicates a greater susceptibility to moisture and potential deterioration over time. In this study, the sorptivity

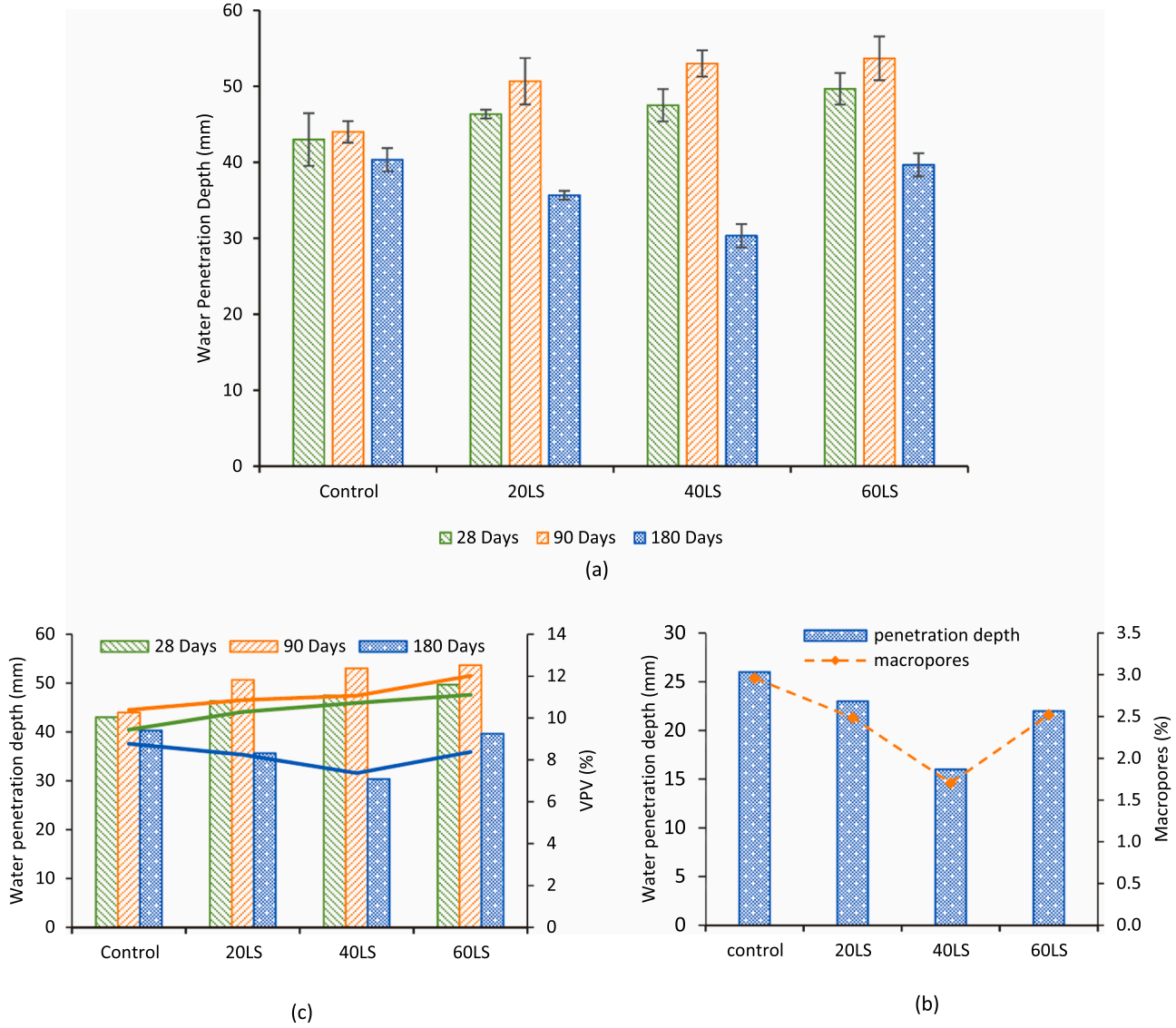

Fig. 14. (a) Water penetration depth of different mixes, comparison of (b) water permeability with VPV test and (c) water permeability with porosity.

coefficients for all mixes were calculated by taking the slope of the initial sorptivity line that fits best by linear regression analysis. All mixes have an R^2 value greater than 0.98 as shown in Fig. 16 (a-d). It is observed that the sorptivity co-efficient value follows the same trend found in the VPV and water penetration depth test as presented before. With the increase of LS content into the concrete, the sorptivity value increased at the initial stage of curing. At 28 days, the sorptivity co-efficient of the control specimen was 30×10^{-3} mm/sec$^{0.5}$ while 20LS, 40LS, and 60LS concretes had the sorptivity coefficient values of 44×10^{-3}, 66×10^{-3} and 80×10^{-3} mm/sec$^{0.5}$, respectively. As proposed by Cement Concrete & Aggregates Australia [4], the sorptivity coefficient surpassed the recommended limit of 27.1×10^{-3} mm/sec$^{0.5}$ in the LS concretes. The higher the LS content, the higher was the sorptivity value, as shown in Fig. 16 (e).

The increased sorptivity of the LS blended concrete at an early age may be attributed to the increased porosity, which supports the findings in the VPV and water penetration results. However, after six months, all the LS concretes exhibited lower sorptivity values than that of control mix. From 28 to 180 days, the sorptivity coefficient of the control specimen decreased only 13.3% while the 20LS, 40LS and 60LS concrete showed 47.7%, 75.7% and 72.5% reduction in sorptivity, respectively. This implies that the sorptivity decreases with the increase of LS content in the concretes at later stage of curing as seen in Fig. 16 (a-d). Therefore, the sorptivity coefficient of all LS concretes are within the allowable limit according to Cement Concrete & Aggregates Australia, 2009 [37]. The presence of LS in concrete results in a significant decrease in sorptivity at late age, which can be directly attributed to the reduction in porosity. This is due to the high concentration of amorphous silica and alumina present in LS, which triggers a pozzolanic reaction and effectively reduces the number of capillary pores. Studies have confirmed that LS consume most of the CH and turns it into C-S-H gel, which then fills up large pores [8,38].

3.7. SEM and EDS analysis

The scanning electron microscope (SEM) and energy dispersive X-ray spectroscopy (EDS) analysis are conducted in this study on all four mixes to investigate the microstructural properties and their variation over time. It is observed that the microstructure of all concrete mixes, including those containing LS, shows improvement over time. However, the variation in transport properties of those mixes can be explained by microstructural analysis. It is well known that the cement paste formed through hydration reaction contains interconnected pores of various sizes, as discussed in the porosity section. Based on the SEM image the

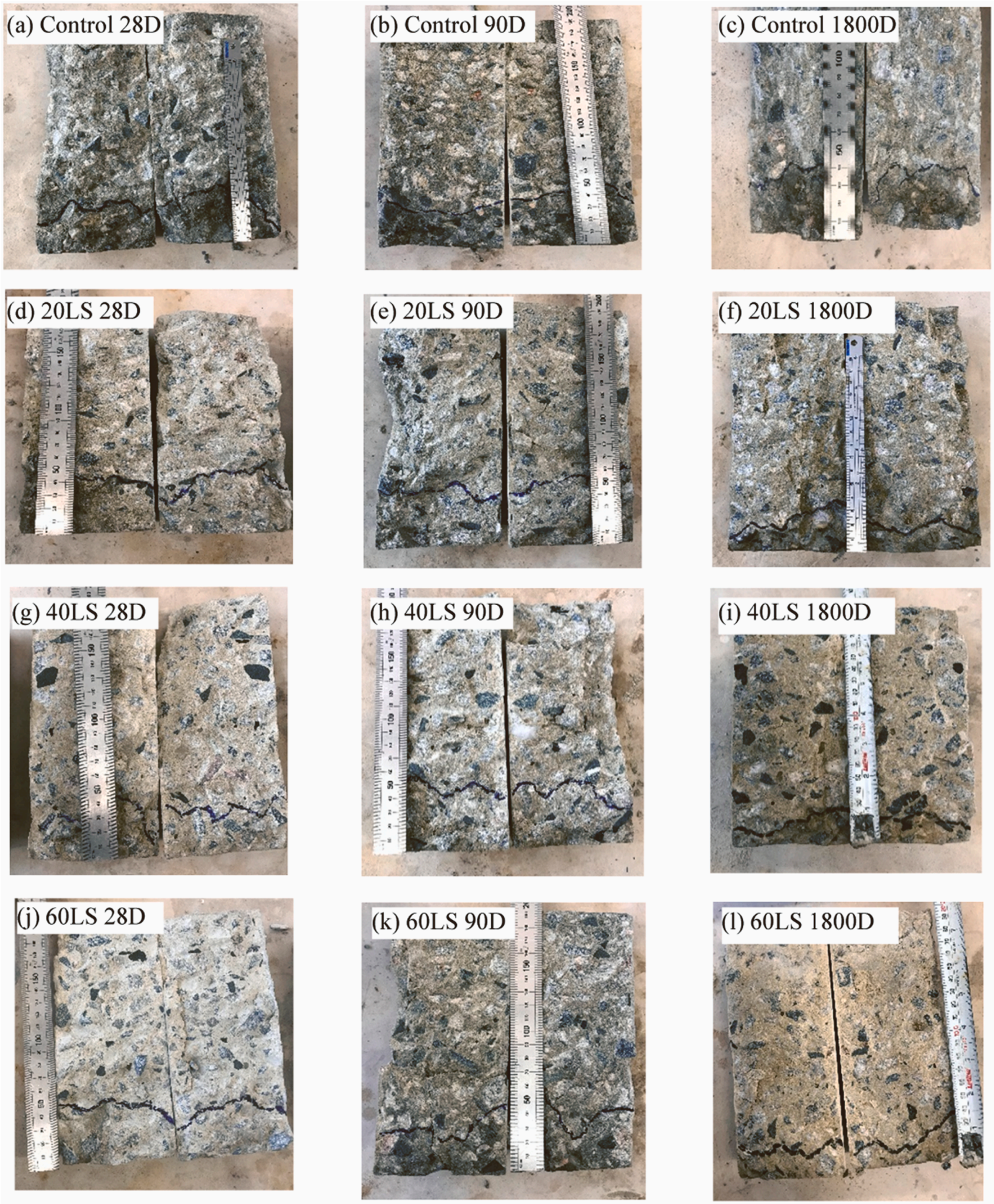

Fig. 15. Water penetration depth of control (a-c), 20LS (d-f), 40LS (g-i) and 60LS (j-l) specimen.

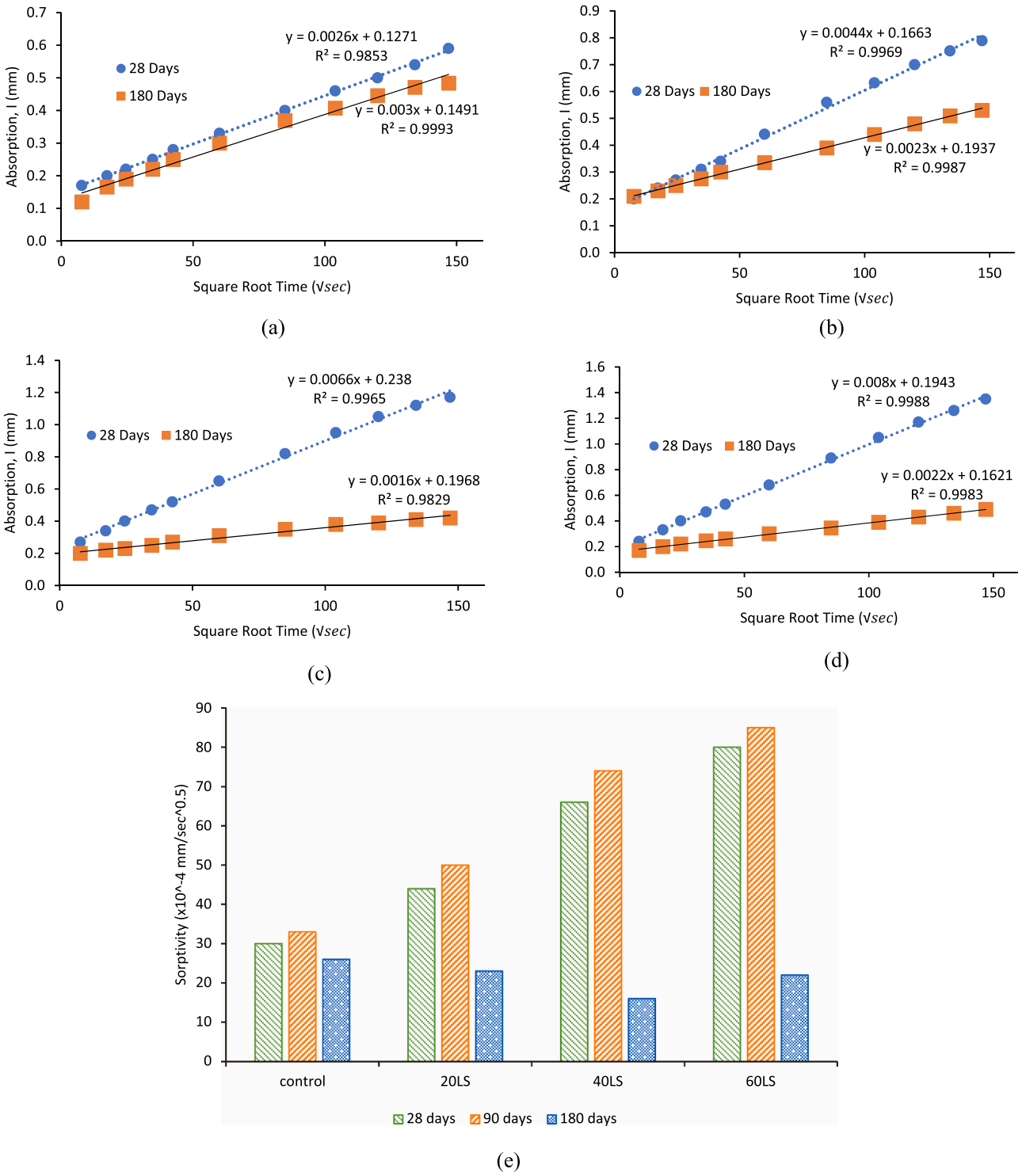

Fig. 16. Initial sorptivity of control (a), 20LS (b), 40LS (c) and 60LS (d) concrete, sorptivity co-efficient (e).

control concrete appears more compact than those of LS-containing concrete as shown in Fig. 17. Furthermore, unreacted LS particles are also observed at early days which primarily act as fillers in 20LS, 40LS, and 60LS concrete presented in Fig. 18. Thus, the addition of LS to concrete as binder increases the porosity in the material, thereby adversely affecting its transport properties during the early age of curing.

In contrast, the microstructures of control concrete become denser as time progresses due to the development of hydration products. This densification is also noticeable in the 20% and 40% LS concrete samples at later ages. It is apparent that the number of capillary and larger pores decreased in samples containing 20% and 40% LS after 6 months of age as shown in Fig. 9 in the porosity analysis part. These pores are surrounded or filled by C-S-H and C-A-S-H gel, resulting from cement hydration and the secondary pozzolanic reaction of LS [17]. Additionally, existing literature suggests that LS particles with a high SO_3 content contribute to the formation of inflatable ettringite (AFt) in an alkaline environment [17]. This extra C-S-H and AFt can also fill large pores of concrete which decreases the total number of pores in LS blended concrete as shown in Fig. 9 (d). It is also evident that the higher the LS

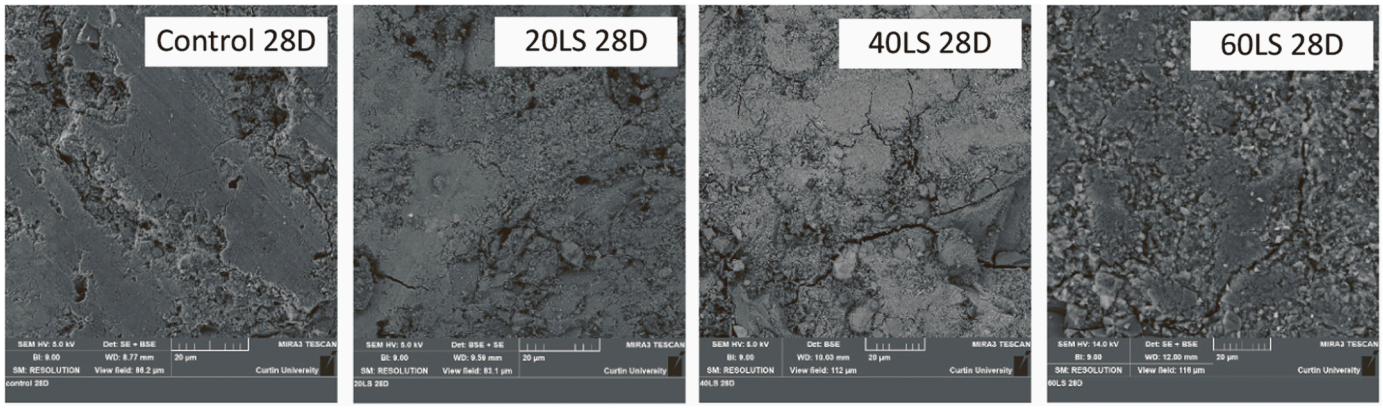

Fig. 17. Concrete surface of four mixes at 28D.

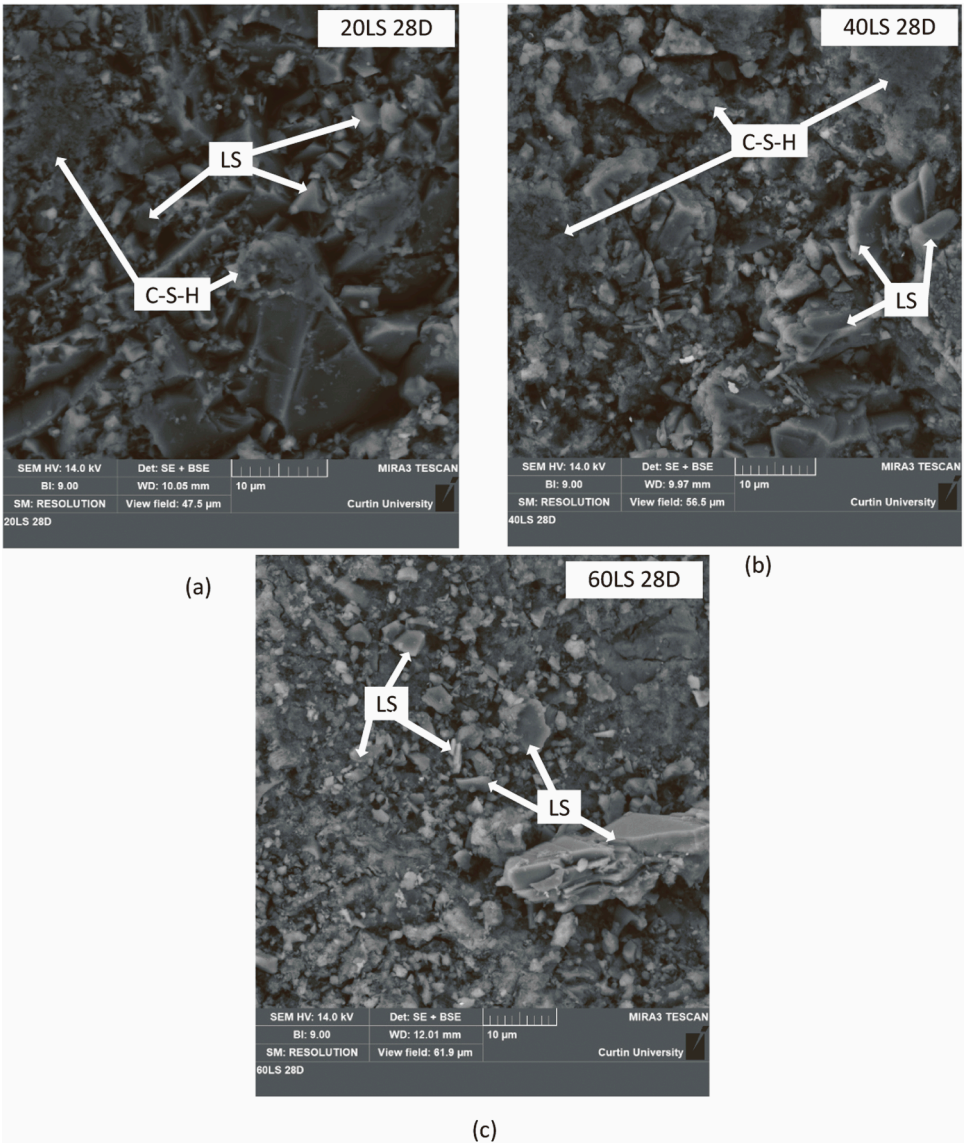

Fig. 18. Unreacted LS particles of LS blended concrete at 28 days (a) 20LS (b) 40LS and (c) 60LS concrete.

content in the binder, the fewer the pores up to 40% replacement by LS which also supports the findings of pore analysis. Moreover, when 40% LS is added to the concrete, the formation of rectangular crystals are observed that grow in a specific direction as seen in Fig. 19 (b). The rectangular shaped crystals are seen near the cracking zone and the higher spectrum of Ca and Oxygen on that crystals from the EDS analysis can be resulted from the calcium carbonate ($CaCO_3$) formation as presented in Fig. 20 (a). This $CaCO_3$ can be formed due to the carbonation

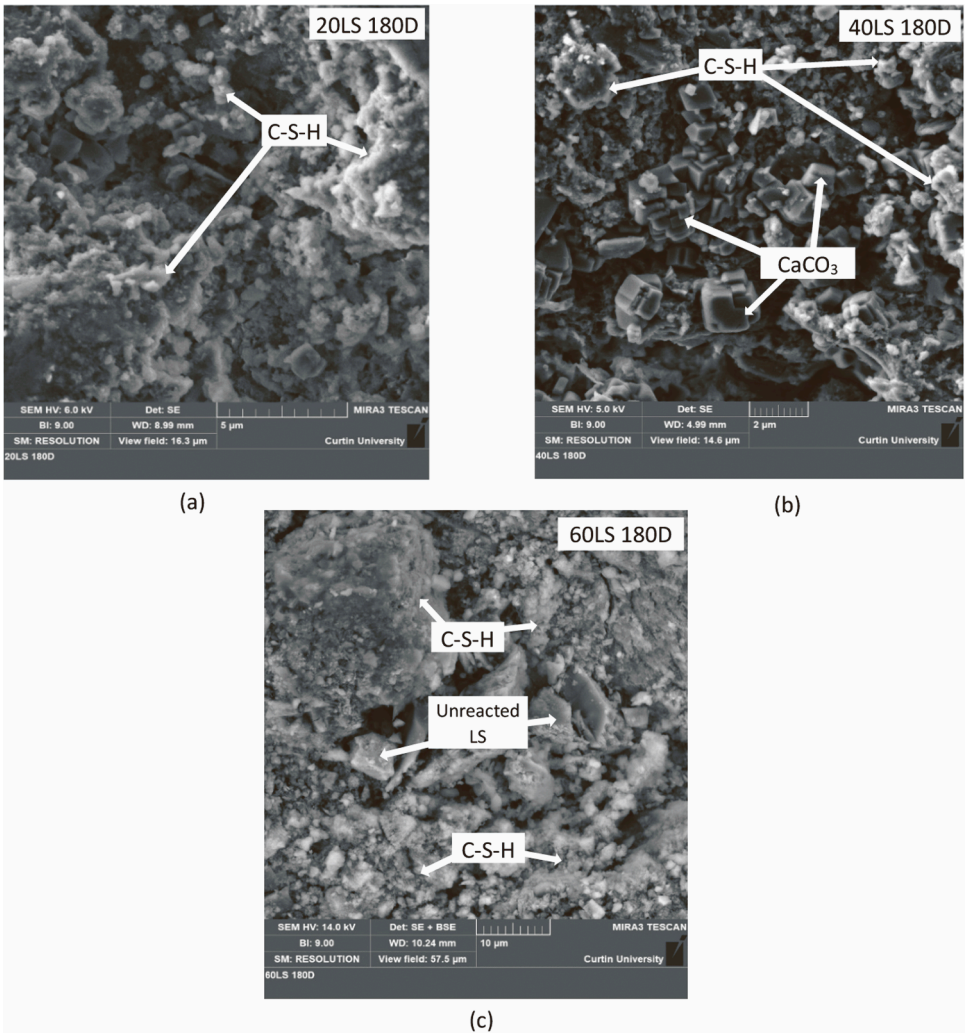

Fig. 19. hydration product of (a) 20LS and 40LS (b) concrete and un-hydrated LS of 60LS concrete (c) at 180 days.

process at later age where the carbon dioxide (CO_2) from the air reacts with calcium hydroxide $Ca(OH)_2$ in the concrete and can produce $CaCO_3$ [39,40]. This may be the reason which significantly reduces the number of pores in 40LS concrete and improves transport properties. These findings align with the improvements observed in various parameters, including VPV, water absorption, and water sorptivity. Therefore, adding 40% LS in concrete generates higher microstructural development among the four mixes.

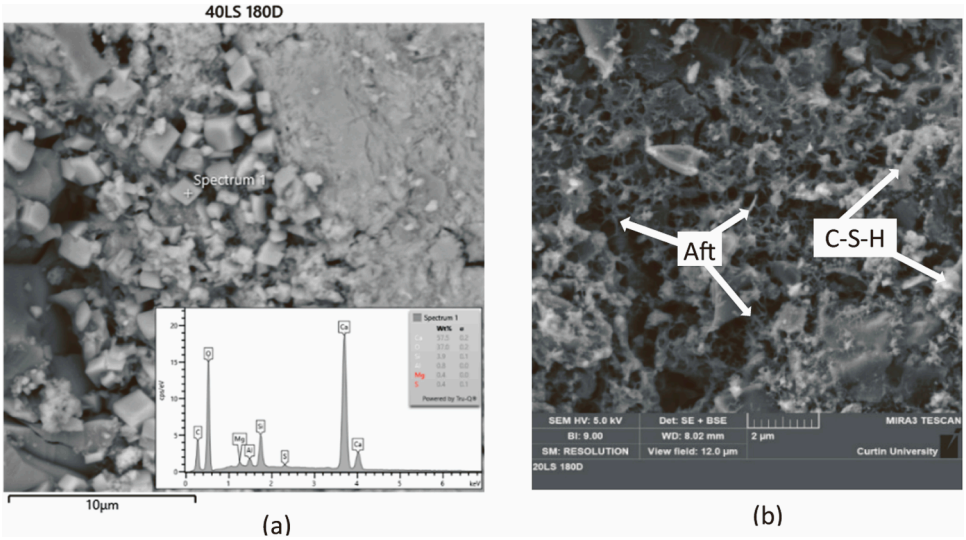

Fig. 20. Formation of $CaCO_3$ (a) and Aft (b) in LS blended concrete.

In contrast, when replacing 60% of cement with LS, there was less improvement in microstructure properties in comparison to the 40% replacement scenario. This can be attributed to the presence of a lower amount of calcium (Ca) content, which leaves unreacted LS particles within the concrete samples depicted in Fig. 19 (c) and does not contribute that much to the pore reduction. Therefore, the size of macropores and total number of pores are higher in 60LS concrete than those in 40LS concrete. These findings are in agreement with the results obtained from VPV, water penetration, water sorptivity, and sorptivity co-efficient presented earlier.

4. Conclusion

The effects of LS on the permeation properties of concrete were studied by using 20%, 40% and 60% cement replacements by LS. The summary of the findings are as follows:

1. The incorporation of LS as SCM in concrete leads to an improvement in compressive strength up to 40% cement replacement, though strength development was relatively slow at early days due to delayed activation of LS. However, 40% replacement exhibited the highest compressive strength among all four mixes after 6 months of age.
2. LS significantly refines the pore structure of concrete. Although there was a slight increase in both gel pores and larger pores after 28 days of curing, a significant reduction in macro porosity was observed after 180 days, leading to improvements in the transport properties of concrete.
3. The use of LS significantly decreases the VPV, water penetration depth and sorptivity of concrete. Because of having least macro-porosity and higher compressive strength, 40% replacement has shown the least value among four mixes after 6 months of age.
4. The microstructure analysis revealed that the addition of 20% LS resulted in the formation of C-S-H and C-A-S-H gel, leading to the expected improvements in strength and porosity. However, at 60% replacements, unreacted LS particles are observed due to the insufficient Ca content in the mix. Consequently, increasing the LS replacement beyond a certain threshold showed decline in concrete properties.

CRediT authorship contribution statement

Shaikh Faiz Ahmed: Writing – review & editing, Supervision, Project administration, Funding acquisition. **Amin Md Tanvir Ehsan:** Writing – original draft, Visualization, Validation, Methodology, Formal analysis, Data curation, Conceptualization. **Sarker Prabir Kumar:** Writing – review & editing, Supervision, Project administration, Funding acquisition.

Declaration of Competing Interest

The authors declare that they have no known competing financial interests or personal relationships that could have appeared to influence the work reported in this paper.

Data availability

Data will be made available on request.

Acknowledgment

The authors would like to acknowledge Australian Research Council (ARC), Australia for providing financial support in this research (Discovery Project grant DP200102784). The authors also acknowledge the use of Scanning Electron Microscope (Tescan MIRA), at John De Laeter Centre at Curtin University, Australia.

References

[1] P. Nath, P. Sarker, Effect of fly ash on the durability properties of high strength concrete, Procedia Eng. 14 (2011) 1149–1156, https://doi.org/10.1016/j.proeng.2011.07.144.
[2] G. Adil, J.T. Kevern, D. Mann, Influence of silica fume on mechanical and durability of pervious concrete, Constr. Build. Mater. 247 (2020) 118453, https://doi.org/10.1016/j.conbuildmat.2020.118453.
[3] I. Arribas, I. Vegas, J.T. San-José, J.M. Manso, Durability studies on steelmaking slag concretes, Mater. Des. 63 (2014) 168–176, https://doi.org/10.1016/j.matdes.2014.06.002.
[4] Q. Wang, P. Yan, J. Yang, B. Zhang, Influence of steel slag on mechanical properties and durability of concrete, Constr. Build. Mater. 47 (2013) 1414–1420, https://doi.org/10.1016/j.conbuildmat.2013.06.044.
[5] B.S. Divsholi, T.Y.D. Lim, S. Teng, Durability properties and microstructure of ground granulated blast furnace slag cement concrete, Int. J. Concr. Struct. Mater. 8 (2014) 157–164, https://doi.org/10.1007/s40069-013-0063-y.
[6] P. Duan, Z. Shui, W. Chen, C. Shen, Enhancing microstructure and durability of concrete from ground granulated blast furnace slag and metakaolin as cement replacement materials, J. Mater. Res. Technol. 2 (2013) 52–59, https://doi.org/10.1016/j.jmrt.2013.03.010.
[7] J. Li, P. Lian, S. Huang, L. Huang, Recycling of lithium slag extracted from lithium mica by preparing white Portland cement, J. Environ. Manag. 265 (2020) 110551, https://doi.org/10.1016/j.jenvman.2020.110551.
[8] Z. hai He, S. gui Du, D. Chen, Microstructure of ultra high performance concrete containing lithium slag, J. Hazard. Mater. 353 (2018) 35–43, https://doi.org/10.1016/j.jhazmat.2018.03.063.
[9] M.U. Hossain, C.S. Poon, Y.H. Dong, D. Xuan, Evaluation of environmental impact distribution methods for supplementary cementitious materials, Renew. Sustain. Energy Rev. 82 (2018) 597–608, https://doi.org/10.1016/j.rser.2017.09.048.
[10] E. and R. Department of Industry, Science, Mineral Commodity Summaries 2022, 2022. https://publications.industry.gov.au/publications/resourcesandenergyquarterlymarch2022/index.html.
[11] H. Tan, X. Zhang, X. He, Y. Guo, X. Deng, Y. Su, J. Yang, Y. Wang, Utilization of lithium slag by wet-grinding process to improve the early strength of sulphoaluminate cement paste, J. Clean. Prod. 205 (2018) 536–551, https://doi.org/10.1016/j.jclepro.2018.09.027.
[12] T. Zhang, B. Ma, H. Tan, X. Liu, P. Chen, Z. Luo, Effect of TIPA on mechanical properties and hydration properties of cement-lithium slag system, J. Environ. Manag. 276 (2020) 111274, https://doi.org/10.1016/j.jenvman.2020.111274.
[13] T. Wu, S.T. Ng, J. Chen, Deciphering the CO_2 emissions and emission intensity of cement sector in China through decomposition analysis, J. Clean. Prod. 352 (2022) 131627, https://doi.org/10.1016/j.jclepro.2022.131627.
[14] L. Qi, H. Shaowen, Z. Yuxuan, L. Jinyang, P. Weiliang, W. Yufeng, Influence of lithium slag from lepidolite on the durability of concrete, IOP Conf. Ser. Earth Environ. Sci. 61 (2017), https://doi.org/10.1088/1755-1315/61/1/012151.
[15] H. Tan, M. Li, X. He, Y. Su, J. Yang, H. Zhao, Effect of wet grinded lithium slag on compressive strength and hydration of sulphoaluminate cement system, Constr. Build. Mater. 267 (2021) 120465, https://doi.org/10.1016/j.conbuildmat.2020.120465.
[16] S.A. Rahman, F.U.A. Shaikh, P.K. Sarker, A comprehensive review of properties of concrete containing lithium refinery residue as partial replacement of cement, Constr. Build. Mater. 328 (2022) 127053, https://doi.org/10.1016/j.conbuildmat.2022.127053.
[17] Z. hai He, L. yuan Li, S. gui Du, Mechanical properties, drying shrinkage, and creep of concrete containing lithium slag, Constr. Build. Mater. 147 (2017) 296–304, https://doi.org/10.1016/j.conbuildmat.2017.04.166.
[18] W. Yiren, W. Dongmin, C. Yong, Z. Dapeng, L. Ze, Micro-morphology and phase composition of lithium slag from lithium carbonate production by sulphuric acid process, Constr. Build. Mater. 203 (2019) 304–313, https://doi.org/10.1016/j.conbuildmat.2019.01.099.
[19] J. Li, S. Huang, Recycling of lithium slag as a green admixture for white reactive powder concrete, J. Mater. Cycles Waste Manag. 22 (2020) 1818–1827, https://doi.org/10.1007/s10163-020-01069-4.
[20] H. Bahmani, D. Mostofinejad, Microstructure of ultra-high-performance concrete (UHPC) – A review study, J. Build. Eng. 50 (2022), https://doi.org/10.1016/j.jobe.2022.104118.
[21] H. Tan, M. Li, X. He, Y. Su, J. Zhang, H. Pan, J. Yang, Y. Wang, Preparation for micro-lithium slag via wet grinding and its application as accelerator in Portland cement, J. Clean. Prod. 250 (2020) 119528, https://doi.org/10.1016/j.jclepro.2019.119528.
[22] Y. He, Q. Zhang, Q. Chen, J. Bian, C. Qi, Q. Kang, Y. Feng, Mechanical and environmental characteristics of cemented paste backfill containing lithium slag-blended binder, Constr. Build. Mater. 271 (2021) 121567, https://doi.org/10.1016/j.conbuildmat.2020.121567.
[23] M. Zhai, J. Zhao, D. Wang, Y. Wang, Q. Wang, Hydration properties and kinetic characteristics of blended cement containing lithium slag powder, J. Build. Eng. 39 (2021) 102287, https://doi.org/10.1016/j.jobe.2021.102287.
[24] H. Tan, X. Li, C. He, B. Ma, Y. Bai, Z. Luo, Utilization of lithium slag as an admixture in blended cements: physico-mechanical and hydration characteristics, J. Wuhan. Univ. Technol. Mater. Sci. Ed. 30 (2015) 129–133, https://doi.org/10.1007/s11595-015-1113-x.
[25] F.F. Wu, K.Bin Shi, S.K. Dong, Influence of concrete with lithium-slag and steel slag by early curing conditions, Key Eng. Mater. 599 (2014) 52–55, https://doi.org/10.4028/www.scientific.net/KEM.599.52.

[26] B. Li, R. Cao, N. You, C. Chen, Y. Zhang, Products and properties of steam cured cement mortar containing lithium slag under partial immersion in sulfate solution, Constr. Build. Mater. 220 (2019) 596–606, https://doi.org/10.1016/j.conbuildmat.2019.06.062.
[27] S.M.A. Rahman, A.H. Mahmood, F.U.A. Shaikh, P.K. Sarker, Fresh state and hydration properties of high-volume lithium slag cement composites, Mater. Struct. Constr. 56 (2023) 1–19, https://doi.org/10.1617/s11527-023-02177-x.
[28] F.U.A. Shaikh, S.W.M. Supit, Mechanical and durability properties of high volume fly ash (HVFA) concrete containing calcium carbonate (CaCO3) nanoparticles, Constr. Build. Mater. 70 (2014) 309–321, https://doi.org/10.1016/j.conbuildmat.2014.07.099.
[29] H.F.W. Taylor, Cem. Chem. (1997), https://doi.org/10.1680/cc.25929.
[30] R. Abousnina, A. Manalo, W. Ferdous, W. Lokuge, B. Benabed, K. Saif Al-Jabri, Characteristics, strength development and microstructure of cement mortar containing oil-contaminated sand, Constr. Build. Mater. 252 (2020) 119155, https://doi.org/10.1016/j.conbuildmat.2020.119155.
[31] A.M. Awedat, Y. Zhu, J.M.L. Bennett, S.R. Raine, The impact of clay dispersion and migration on soil hydraulic conductivity and pore networks, Geoderma 404 (2021) 115297, https://doi.org/10.1016/j.geoderma.2021.115297.
[32] S.M.A. Rahman, A.H. Mahmood, F.U.A. Shaikh, P.K. Sarker, Fresh state and hydration properties of high-volume lithium slag cement composites, Mater. Struct. Constr. 56 (2023) 1–19, https://doi.org/10.1617/s11527-023-02177-x.
[33] R. Kumar, B. Bhattacharjee, Porosity, pore size distribution and in situ strength of concrete, Cem. Concr. Res. 33 (2003) 155–164, https://doi.org/10.1016/S0008-8846(02)00942-0.
[34] M. Yudenfreund, K.M. Hanna, J. Skalny, I. Older, S. Brunauer, Hardened Portland cement pastes of low porosity V. Compressive strength, Cem. Concr. Res. 2 (1972) 731–743, https://doi.org/10.1016/0008-8846(72)90008-7.
[35] VicRoad, Technical Note 89: Test Methods for the Assessment of Durability of Concrete, 3 (2007) 1–4.
[36] R. Abousnina, A. Manalo, W. Lokuge, Z. Zhang, Effects of light crude oil contamination on the physical and mechanical properties of geopolymer cement mortar, Cem. Concr. Compos. 90 (2018) 136–149, https://doi.org/10.1016/j.cemconcomp.2018.04.001.
[37] Cement Concrete & Aggregates, Chloride Resistance of Concrete, Cem. Concr. Aggregates Aust. (2009) 1–37.
[38] Y. He, S. Liu, R.D. Hooton, X. Zhang, S. He, Effects of TEA on rheological property and hydration performance of lithium slag-cement composite binder, Constr. Build. Mater. 318 (2022) 125757, https://doi.org/10.1016/j.conbuildmat.2021.125757.
[39] H. Choi, M. Inoue, R. Sengoku, Change in crystal polymorphism of CaCO3 generated in cementitious material under various pH conditions, Constr. Build. Mater. 188 (2018) 1–8, https://doi.org/10.1016/j.conbuildmat.2018.08.045.
[40] K. Samimi, S. Kamali-Bernard, A.A. Maghsoudi, Durability of self-compacting concrete containing pumice and zeolite against acid attack, carbonation and marine environment, Constr. Build. Mater. 165 (2018) 247–263, https://doi.org/10.1016/j.conbuildmat.2017.12.235.